Post-Synthetic Thiol-Induced Reshaping of Copper Sulfide Nanoparticles

Haley L. Young,[1] Connor R. McCormick,[1] Auston G. Butterfield,[1] Enrique D. Gomez,[2,3,4] and Raymond E. Schaak[1,2,4,*]

[1] *Department of Chemistry*, [2] *Department of Chemical Engineering*, [3] *Department of Materials Science and Engineering*, and [4] *Materials Research Institute*, *The Pennsylvania State University, University Park, Pennsylvania 16802, United States*

E-mail: res20@psu.edu

Abstract

Nanoparticles of copper sulfide, including roxbyite $Cu_{1.8}S$, are important materials for many applications and they also serve as versatile templates for cation exchange reactions that transform them into derivative metal sulfide compounds and complex heterostructures. The sizes and shapes of roxbyite nanoparticles are generally determined during synthesis and their morphologies are retained during post-synthetic modifications such as cation exchange. Here, we demonstrate post-synthetic morphological modification of roxbyite nanoparticles by treating them with 1-dodecanethiol (1-DDT) and *tert*-dodecanethiol (t-DDT) at temperatures ranging from 90 °C to 160 °C. These thiols, which are typically used as ligands and/or sulfur reagents in nanoparticle synthesis, induce morphological reshaping while maintaining composition, crystal structure, and particle volume. For example, 56 × 21 nm roxbyite nanorods transform to 32 nm spherical particles in the presence of 1-DDT at 130 °C for two or more hours. The nanorods progressively decrease in length and increase in width, forming a series of ellipsoids having tunable aspect ratios at intermediate time points. Control experiments point to a single crystal–to–single crystal pathway that involves material diffusion and migration, which can be accelerated by increasing the density of cation vacancies in the nanoparticles. Because of this pathway, the thiol-induced morphology changes are selective to the copper sulfide regions of heterostructured nanorods containing roxbyite and ZnS, Co_9S_8, or $CuInS_2$ made using partial cation exchange reactions, providing access to a library of derivative nanoparticles having otherwise inaccessible morphologies.

Introduction

Synthetic control of nanoparticle shape and morphology is important for controlling a wide range of functions, including the optical, photophysical, catalytic, and electronic properties that are foundational for their applications in areas that include medicine, energy, and the environment.[1–3] Control over morphology in solution-based colloidal synthesis is often achieved by adding different ligands during synthesis that preferentially interact with different crystal facets to modulate growth.[4–6] Ligands also stabilize the high-energy surfaces of nanoparticles, preventing aggregation and enabling dispersibility.[7] Morphology control can also be achieved by changing reaction parameters, such as metal reagent, reactant concentration, time, and temperature.[8–11] Here, precursor concentration impacts nucleation before particle growth commences, typically at elevated temperatures. Nanoparticle morphology control can also be achieved post-synthetically by altering the shape of the particle after it has already been formed.[12–14] Methods such as irradiation, sintering, or etching can be thought of as adding or subtracting atoms from the particles, forming a shape that would otherwise not be synthesized directly.[14–16]

Copper sulfide is an important nanoparticle system for achieving morphology control, including roxbyite $Cu_{1.8}S$, which is a well-known plasmonic material.[17,18] Several different shapes and sizes of colloidal copper sulfide nanoparticles have been synthesized through variation of copper precursor reactivity, sulfur source, reaction time, temperature, and capping ligands.[11] Among the most common shapes, copper sulfide spheres up to 20 nm in diameter, rods from 30-80 nm in length, and plates up to 130 nm in width have been synthesized.[11,19–21] Being a vacancy rich material, roxbyite copper sulfide nanoparticles, as well as other copper sulfides, have been important for studying photoactivity, including the dependence of photoactivity on morphology.[22] For example, when the absorption of covellite copper sulfide (CuS) spheres, cubes, cuboctahedra, and truncated octahedra were compared, cubes exhibited the strongest absorbance in the near infrared region, which translated to having the most potent photothermal and therapeutic performance.[22] In another case, the near-infrared (NIR) absorption of roxbyite nanodisks could be affected by the size of the particles as well as through plasmonic coupling of the particles in assembled face-to-face structures, demonstrating potential utility in plasmonic applications like sensing and catalysis.[17]

Nanoparticles of copper sulfide are also well-known templates for post-synthetic composition modifications, including through cation exchange reactions.[23,24] For copper sulfides, including roxbyite, copper cations in the nanoparticle are replaced with solubilized cations, such as Zn^{2+} and Co^{2+}, while the anion sublattice structure and the nanoparticle morphology are typically retained.[25] Complete cation exchange can be performed to fully replace the copper cations to yield completely different metal chalcogenide nanoparticles, *i.e.*, ZnS and CoS, with unique morphologies.[20] Alternatively, partial cation exchange reactions only replace some of the copper cations in the nanoparticles, producing heterostructured nanoparticles composed of multiple metal chalcogenide materials and interfaces that have unique properties relevant to applications in catalysis and photovoltaic technologies.[26] Copper sulfide nanoparticles are also known to undergo post-synthetic morphology transformations, although examples remain limited.[11,27] Reacting heterostructured nanoparticles that contain copper sulfide regions with trioctylphosphine (TOP) in the presence of oxygen selectively etches the copper sulfide regions, either sculpting them into narrower shapes through partial removal or completely removing them to create voids.[13,14] The phosphine acts as a reducing agent to remove sulfur from the structure via binding with TOP, leaving the Cu^{+} susceptible to oxidation and solubilization. In another instance, the migration of cation exchange induced defects in biconcave $Cu_{2-x}S$ plates resulted in a slight

morphology change to thick nanoplates.[28]

Ligand exchange, which replaces the ligands on the surfaces of nanoparticles with ligands in solution, is often used to control the dispersibility and stability of nanoparticles in different media and is often a necessary step that precedes downstream surface functionalization.[29–32] However, ligand exchange has also been shown to induce morphology changes, including for copper sulfide nanoparticles. For example, replacing 1-dodecanthiol with 1,2-hexadecanediol on low chalcocite nanospheres at 220 °C led to oriented attachment of the particles to form rods.[12] Similarly, one-dimensional (1-D) copper sulfide nanorods were found to form 2-D structures through etching induced oriented attachment at the rod tips when exposed to an excess amount of hexylphosphonic acid.[33] In a different case, 1-dodecanethiol was used to transform hexagonal nanoplates of covellite (CuS) into thicker, rounded high chalcocite (Cu_2S) nanoplates, which involved both a composition and a shape change.[34] The hexagonal shape and covellite crystal structure could be restored again using an oleic acid-sulfur complex while maintaining the thickness.[34] In this process, 1-dodecanthiol breaks the disulfide bonds of the initial covellite nanoparticles and removes sulfur, and then the oleic acid-sulfur complex adds sulfur back into the system to re-form the disulfide bonds to give the stoichiometric covellite copper sulfide phase. These examples point to the potential utility of post-synthetic ligand exchange for modifying the shapes and sizes of copper sulfide nanoparticles, which is complementary to direct synthesis methods. However, existing capabilities have been limited to a small number of systems and morphologies, and are often accompanied by significant changes in composition. Given the role of size- and shape-controlled copper sulfide nanoparticles as morphological, compositional, and structural templates for a wide range of heterostructured nanoparticles, an expanded portfolio of approaches for achieving post-synthetic morphology changes is desirable.

Here, we show that nanorods of roxbyite copper sulfide, $Cu_{1.8}S$, transform in solution to a library of eight different shapes – including various types of spheres, ellipsoids, and rods – upon exposure to two common thiol reagents, 1-dodecanethiol (1-DDT) and *tert*-dodecanethiol (t-DDT), at temperatures between 90 °C and 160 °C. The vacancy-rich character of roxbyite copper sulfide relative to other metal chalcogenide materials makes it an ideal material to facilitate thiol-driven morphological changes. These morphological changes are classified as single crystal–to–single crystal transformations because of their crystallographic relationships and they occur with retention of particle volume. Roxbyite nanorods are routinely synthesized as uniform particles in high yield, and these characteristics translate to high uniformity and yield of the derivative nanoparticles, many of which represent sizes and/or shapes that have not been accessible for $Cu_{1.8}S$ using direct synthetic methods. When applied to heterostructured nanorods containing roxbyite and a different metal sulfide phase ($Cu_{1.8}S$–ZnS, $Cu_{1.8}S$–Co_9S_8, $Cu_{1.8}S$–$CuInS_2$), morphological reshaping is selective to the vacancy-rich copper sulfide regions. These transformations produce derivative heterostructured nanoparticles with complex morphologies, including compositionally and morphologically asymmetric heterodimers. The experimental insights into thiol-induced morphology changes described here can therefore be merged with the extensive library of cation exchange reactions to access heterostructured nanoparticles with exceptionally complex shapes and compositions.

Experimental Section

Chemicals

1-dodecanethiol (1-DDT, Sigma Aldrich, ≥98%), *tert*-dodecanethiol (t-DDT, Sigma-Aldrich, mixture of isomers, ≥98.5%), isopropyl alcohol (IPA, Millipore), ethanol (Koptec), toluene (Millipore), tetrahydrofuran (THF, anhydrous, Sigma-Aldrich, ≥99.9%), octadecene (ODE, Sigma-Aldrich, 90%), oleylamine (OLAM, Sigma-Aldrich, 70%), benzyl ether (BE, ThermoScientific, 99%), trioctylphosphine oxide (TOPO, Sigma-Aldrich, 98%), trioctylphosphine (TOP, Sigma-Aldrich, ≥99%), tetrachloroethylene (Sigma-Aldrich, ≥99%) copper (II) nitrate trihydrate ($Cu(NO_3)_2 \cdot 3H_2O$, Sigma-Aldrich, ≥99%), iodine (I_2, Mallinckrodt Chemicals), octadecanethiol (ODT, Sigma-Aldrich, 98%), decanethiol (DT, Alfa Aesar, 96%), zinc chloride ($ZnCl_2$, anhydrous, Sigma-Aldrich, 97%), indium chloride ($InCl_3$, anhydrous, Alfa Aesar, ≥98%), and cobalt(II) chloride ($CoCl_2$, purum p.a., Sigma-Aldrich, 97%). All chemicals were used as received without further purification.

Synthesis of roxbyite ($Cu_{1.8}S$) nanorods

In a 250-mL, 3-neck round bottom flask, $Cu(NO_3)_2 \cdot 3H_2O$ (843 mg), TOPO (8.7 g), ODE (45 mL), and OLAM (750 µL) were placed under vacuum. While under vacuum, the temperature was raised to 80 °C and held for 30 minutes. The flask was cycled with a blanket of Ar three times, for approximately two minutes each. Using a syringe, a 22.5 mL mixture of 10:1 t-DDT:1-DDT was rapidly injected into the flask. (All injections were performed manually, not with a syringe pump.) The reaction was placed under Ar flow and the temperature was raised to 180 °C within 5 minutes. The reaction was held at 180 °C for 15 minutes and then removed from heat and cooled with a room temperature water bath. The product was precipitated with 1:1 IPA:acetone and washed by centrifugation and resuspension in toluene three times.[26]

Synthesis of roxbyite ($Cu_{1.8}S$) nanoplates

$Cu(acac)_2$ (0.3926 g), 1-DDT (5 mL), and OLAM (10 mL) were added to a 50 mL, 3-neck round bottom flask and placed under vacuum for 1 hour. The flask was then cycled with Ar three times and slowly heated to 250 °C. The reaction was allowed to stir for 1 hour before precipitating the particles with IPA and washing by centrifugation and resuspension in toluene three times.[35]

Preparation of cation exchange solutions

Cation exchange solutions of 0.018 mmol/mL Co^{2+}, 0.073 mmol/mL Zn^{2+}, and 0.012 mmol/mL In^{3+} were made according to the procedure detailed in reference 26.[26] Briefly, 15 mL of BE, 8 mL of OLAM, 2 mL of ODE, and the desired metal salt (250 mg $ZnCl_2$, 59.6 mg $CoCl_2$, or 67.6 mg $InCl_3$) were added to a 50 mL, 3-neck round bottom flask. The flask was placed under vacuum and heated to 100 °C for 1 hour. The flask was cycled with Ar three times and heated to 200 °C for 30 minutes. The solutions were cooled and stored in septum capped vials.

Synthesis of ZnS nanorods by cation exchange

To obtain ZnS nanorods, cation exchange using a two-fold excess of Zn^{2+} was performed on $Cu_{1.8}S$ nanorods. Briefly, 7.5 mL of BE, 1 mL of ODE, 4 mL of OLAM, and 1.889 mL (excess) Zn^{2+} exchange solution were added to a 50 mL, 3-neck round bottom flask. The flask was heated to 100 °C for 30 minutes. The flask was cycled with Ar three times and heated to 120 °C. In a separate septum-capped vial, 20 mg of $Cu_{1.8}S$ rods were sonicated in 3 mL of TOP for 45 minutes and then

injected into the hot flask. The reaction was run for 30 minutes before the particles were precipitated with 1:1 IPA:ethanol and washed by centrifugation and resuspension in toluene three times.[26]

Preparation of OLAM-S complex

The OLAM-S complex solution was prepared by heating 5 mL of OLAM and 0.5 mmol sulfur powder to 40 °C for 20 minutes. The resulting orange-colored solution was allowed to cool before being used directly in the reaction to make covellite plates.[34]

Synthesis of 50% exchanged nanorod heterostructures

To obtain 50% exchanged $Cu_{1.8}S$ rods, 7.5 mL of BE, 1 mL of ODE, 4 mL of OLAM, and the desired cation exchange solution (1.913 mL Co^{2+} solution, 0.472 mL Zn^{2+} solution, or 1.913 mL In^{3+} solution) were added to a 50 mL, 3-neck round bottom flask. The flask was heated to 100 °C for 30 minutes. The flask was cycled with Ar three times and heated to 120 °C. In a separate septum-capped vial, 20 mg of $Cu_{1.8}S$ rods were sonicated in 3 mL of TOP for 45 minutes and then injected into the hot flask. The reaction was run for 30 minutes before the particles were precipitated with IPA and washed by centrifugation and resuspension in toluene three times.[26]

Synthesis of single tip ZnS–$Cu_{1.8}S$ nanorod heterostructures

Single tip ZnS–$Cu_{1.8}S$ nanorod heterostructures were prepared by heating 7.5 mL of BE, 1 mL of ODE, 4 mL of OLAM, and 0.236 mL Zn^{2+} exchange solution in a 50 mL, 3-neck round-bottom flask under vacuum at 100 °C for 30 minutes. The flask was cycled with Ar three times and heated to 120 °C. In a separate septum-capped vial, 20 mg of $Cu_{1.8}S$ rods were sonicated in 3 mL of TOP for 45 minutes and then injected into the hot flask. The reaction was run for 30 minutes before the flask was cooled in a water bath. The particles were precipitated with IPA and washed by centrifugation and resuspension in toluene three times.[26]

Synthesis of central band $Cu_{1.8}S$–ZnS–$Cu_{1.8}S$ nanorod heterostructures

Central band $Cu_{1.8}S$–ZnS–$Cu_{1.8}S$ nanorod heterostructures were prepared by heating 7.5 mL of BE, 1 mL of ODE, and 4 mL of OLAM in a 50 mL, 3-neck round-bottom flask under vacuum at 100 °C for 30 minutes. The flask was cycled with Ar three times and heated to 120 °C. In a separate septum-capped vial, 20 mg of $Cu_{1.8}S$ rods cycled with Ar were sonicated in 1.75 mL of TOP for 45 minutes and then injected into the hot flask. The temperature was held at 120 °C for 10 minutes before the flask was cooled to room temperature. The Zn^{2+} exchange solution (0.236 mL) was quickly injected and the temperature was ramped up to 100 °C at a rate of 10 °C/min. The reaction was run for 30 minutes before the flask was cooled in a water bath. The particles were precipitated with IPA and washed by centrifugation and resuspension in toluene three times.[26]

Synthesis of double tip ZnS–$Cu_{1.8}S$–ZnS nanorod heterostructures

Double tip ZnS–$Cu_{1.8}S$–ZnS nanorod heterostructures were prepared by heating 250 mg of $ZnCl_2$, 15 mL of BE, 2 mL of ODE, and 8 mL of OLAM in a 50 mL, 3-neck round-bottom flask under vacuum at 100 °C for 30 minutes. The flask was cycled with Ar three times and heated to 200 °C where it was held for 30 minutes. The solution was cooled to 50 °C. In a separate septum-capped vial, 20 mg of $Cu_{1.8}S$ rods cycled with Ar were sonicated in 3 mL of TOP for 45 minutes and then injected into the flask. The reaction ran for 45 minutes before the flask was cooled with a water

bath. The particles were precipitated with 1:1 IPA:ethanol and washed by centrifugation and resuspension in toluene three times.[26]

Additional Zn^{2+} exchange of 1-DDT treated nanorod heterostructures

The following procedure was used for fully exchanging Zn^{2+} in the 1-DDT treated double tip, central band, and single tip nanorod heterostructures. Briefly, 7.5 mL of BE, 1 mL of ODE, 4 mL of OLAM, and the a twofold excess Zn^{2+} cation exchange solution (0.944 mL) were added to a 50 mL, 3-neck round bottom flask. The flask was heated to 100 °C for 30 minutes. The flask was cycled with Ar three times and heated to 120 °C. In a separate septum-capped vial, 10 mg of the desired rods were sonicated in 3 mL of TOP for 45 minutes and then injected into the hot flask. The reaction was run for 30 minutes before the particles were precipitated with IPA and washed by centrifugation and resuspension in toluene three times.

I_2 treatment of $Cu_{1.8}S$ rods

$Cu_{1.8}S$ rods (10 mg) were suspended in a vial with 2 mL of THF to make a 5 mg/mL solution. To treat the particles, 100 μL of 0.02 M I_2 in THF were injected into the vial. The vial was sonicated for 5 minutes and then stirred for 15 minutes. The particles were washed and centrifuged with IPA twice followed by ethanol once.[36]

Thiol treatment reactions

All thiol treatment reactions were run under the same conditions with the appropriate ligand (1-DDT, t-DDT, OLAM-S), temperature and time. In general, 7.5 mL of ODE and 1 mL OLAM were added to a 3-neck round bottom flask and placed under vacuum before heating to 100 °C. The temperature was held for 1 hour. The flask was then cycled with a blanket of Ar three times. The solution was adjusted to the desired temperature. In a separate septum-capped vial, 7.5 mg of nanoparticles were dried under vacuum. The desired ligand was then added to the vial and cycled between vacuum and Ar three times. The vial was briefly sonicated to suspend the nanoparticles in the ligand solution. When the round-bottom flask reached the desired temperature, the nanoparticle solution was injected into the flask. The time was immediately started after injection. Tables S1 and S2 in the Supporting Information show the specific conditions used for each thiol treatment reaction.

Characterization

An Empyrean diffractometer was used to collect powder X-ray diffraction (XRD) data using Cu Kα radiation. Samples were prepared by dropcasting on a zero background Si sample holder. Transmission electron microscopy (TEM) images were obtained using a Veleta camera on a FEI Tecnai G20 20 XTWIN microscope operating at 200 kV with a typical dose rate of 26.5 e/Å^{2}s and screen current of 0.70 nA. High-resolution transmission electron microscopy (HRTEM), high-angle annular dark field (HAADF), and scanning transmission electron microscopy energy dispersion spectroscopy (STEM-EDS) images were collected using a Ceta camera and a SuperX EDS detector on a FEI Talos F200X S/TEM at an accelerating voltage of 200 kV with a typical dose rate of 15.9 e/Å^{2}s and screen current of 0.81 nA. A dwell time of 1 μs was used in STEM mode. Ultraviolet-near infrared (UV-NIR) spectra were collected in a quartz cuvette using a Perkin-Elmer Lambda 950 spectrometer using a standard detector and a wavelength range of 500 to 2000 nm, with a data interval of 2 nm. Samples were prepared in tetrachloroethylene and sonicated for 5 minutes directly before measurement.

Results and Discussion

Nanorods of roxbyite copper sulfide ($Cu_{1.8}S$) with dimensions of 56 ± 3 × 21 ± 1 nm were synthesized according to a previously reported method where $Cu(NO_3)_2 \cdot 3H_2O$ and a 10:1 mixture of tert-dodecanethiol:dodecanethiol were reacted at 180 °C for 15 min in octadecene, oleylamine, and trioctylphosphine oxide.[26] Transmission electron microscopy (TEM), high resolution TEM (HRTEM), and powder X-ray diffraction (XRD) data for the roxbyite nanorods are shown in Figure 1. The nanorods were then subjected to treatment with the thiol ligands 1-DDT and t-DDT. Both 1-DDT and t-DDT are common reagents in copper sulfide nanoparticle synthesis, providing a sulfur source through decomposition at elevated temperatures and also acting as stabilizers.[37] Of the two, t-DDT is considered to be the more reactive thiol, as it decomposes at a lower temperature than 1-DDT.[27,37] This difference in reactivity influences the stabilization and growth of different facets, thereby impacting the resulting nanoparticle shape.[11,27] To investigate the impact of thiol exposure post-synthetically, as opposed to during nanoparticle synthesis, the roxbyite nanorods and desired thiol ligand were injected into a heated solution of oleylamine and octadecene, as described in the Experimental Section and as discussed below.

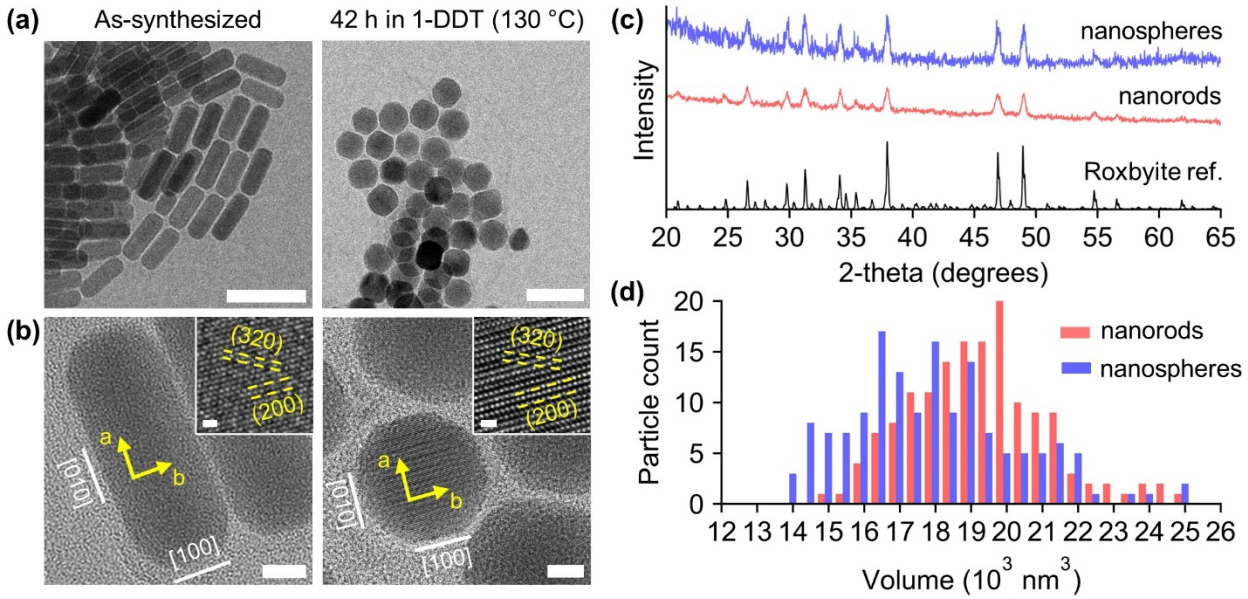

Figure 1. (a) TEM images characterizing the morphology transformation of $Cu_{1.8}S$ rods to spheres using 1-DDT after 42 hours at 130 ºC. Scale bars are 100 nm. (b) HRTEM images of the rods and spheres. Scale bars in the main panels are 10 nm and scale bars in the insets are 1 nm. (c) Experimental powder XRD patterns of the rods and spheres, along with a reference pattern for roxbyite $Cu_{1.8}S$.[38] (d) Histogram showing the particle volumes calculated for the nanorod precursors and nanosphere products.

The roxbyite nanorods were first treated with 1-DDT at 130 °C, conditions comparable to typical ligand exchange reactions. The TEM image in Figure 1 shows that this treatment with 1-DDT transformed the nanorods into multi-faceted, nominally spherical nanoparticles over the course of 42 hours, and the corresponding XRD pattern confirms that the roxbyite crystal phase is retained after the morphology change. The spherical nanoparticles formed after 42 hours of treatment with 1-DDT have an average diameter of 32 ± 2 nm, which represents a 43% decrease in length and a 52% increase in width relative to the nanorods from which they were derived. The

ability to access uniform spherical particles with a diameter of 32 nm is significant because this size range is difficult to target directly and it creates a platform for testing fundamental size-dependent properties, both for roxbyite and for derivative cation-exchanged products. Typical colloidal syntheses produce spherical roxbyite copper sulfide nanoparticles having diameters up to 20 nm.[20,39]

Figure 1d also shows a histogram characterizing and comparing the volumes of the roxbyite nanorods before 1-DDT treatment and the roxbyite nanospheres after 42 hours of 1-DDT treatment generated from TEM images. We measured the lengths and widths of 150 as-synthesized rods and 150 1-DDT-treated spheres and then calculated the corresponding volume of each particle, assuming a perfect cylinder for the nanorods and a perfect sphere for the nominally spherical nanoparticles. While these are idealized geometric estimates that do not take into account faceting, they are reasonable approximations based on the known morphologies of copper sulfide nanorods and spherical nanoparticles.[11,40] Using this process, the average volume and standard deviation of the initial rods was estimated to be $1.9 \times 10^4 \pm 0.2 \times 10^4$ nm^3, while the average volume of the spherical nanoparticles formed by transforming the nanorods was $1.8 \times 10^4 \pm 0.2 \times 10^4$ nm^3. These volumes are considered to be identical, given the standard deviations and the assumptions made in the calculations, and therefore are consistent with a transformation process that reshapes the nanoparticles without involving dissolution and recrystallization, which most likely would not have conserved particle volume.

HRTEM imaging was used to identify the crystallographic relationships between the precursor nanorods and the product nanospheres after 42 hours of 1-DDT treatment. The slightly distorted hexagonally closed packed (200) plane of roxbyite, corresponding to the a-direction of the monoclinic crystal structure, aligns with the length of the nanorod, as seen in Figure 1b. This orientation was identified by comparing the measured 6.5 Å spacing between the lattice planes in the roxbyite nanorods with the d-spacing of 6.7 Å that was expected based on the roxbyite crystal structure.[38] Similarly, the spacing of the (320) plane was similarly measured as 3.4 Å, which compared favorably with the expected value of 3.7 Å. This same (200) plane can also be identified in the spheres obtained after 42 hours of treatment with 1-DDT. Here the d-spacing of the (200) planes was measured as 6.7 Å and the d-spacing of the (320) planes was measured as 3.3 Å. Interestingly, the facets on the tips and edges of the as-synthesized roxbyite nanorods, and the most visible facets on the nominally spherical nanoparticle products, are the same, based on the directions in which the close-packed planes stack. These facets are noted by the white lines in Figure 1b and identified as the [100] and [010] family of planes, respectively. This observation indicates a significant crystallographic relationship between the precursor and product and suggests that the transformation of the nanorods into spheres occurs by decreasing the number of stacked closed packed planes along the length of the particle while increasing the area of the closed packed planes, without disrupting the crystal structure or its orientation within the transforming particle.

To better understand the process by which the morphological reshaping occurred, aliquots were taken to bridge the time during which the morphology changed from nanorods to nanospheres. Figure 2 shows TEM images for this series of samples, along with histograms characterizing the distributions of particle lengths and widths for each sample. The starting nanorods (0 hour time point) have dimensions of 56 ± 3 nm $\times$ 21 ± 1 nm, but by 15 min, the nanorods have started to become shorter and wider with dimensions of 52 ± 4 nm $\times$ 24 ± 1 nm. The nanorods continue to shorten and widen through the 30 min (44 ± 4 nm $\times$ 27 ± 1 nm) and 1

hour (38 ± 3 nm × 30 ± 1 nm) time points, ultimately taking on an elliptical shape during this period. By two hours, the morphology change to nominally spherical particles is complete, yielding dimensions of 33 ± 1 nm × 33 ± 1 nm. Interestingly, with each aliquot (15 min, 30 min, 1 h, 2 h), the width decreases by approximately 3 nm, which represents about 14% of the initial rod width. Given the spacing of the time points, this indicates that longer time intervals are required to change the width by the same amount as the treatment with 1-DDT progresses. The length of the rod similarly experiences a faster change in the early aliquots. By 15 minutes the rod length decreases by approximately 4 nm, which is about 7% of the initial rod length. In another 15 minutes (*i.e.*, the 30 minute aliquot), the rod length decreases an additional 8 nm, which is approximately 14% of the initial rod length. Between 30 minutes and 1 hour, the length decreases an additional 11% (6 nm) and then another 9% (~5 nm) by 2 hours, finally converging to the final width of 33 ± 1 nm, which is identical to the length and therefore corresponds to spherical particles.

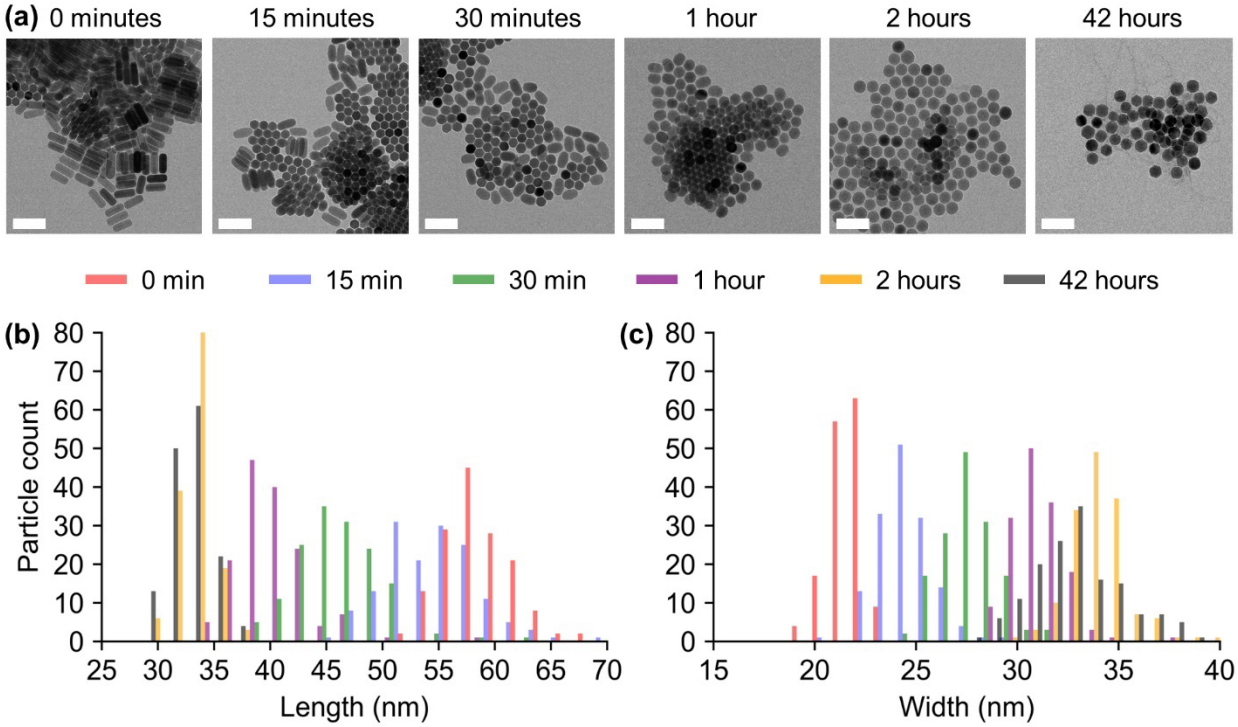

Figure 2. (a) TEM images of aliquots showing the morphology transformation of $Cu_{1.8}S$ rods to spheres using 1-DDT at 130 ºC. Scale bars are 100 nm. Histograms show the (b) lengths and (c) widths for the particles in each aliquot.

We then carried out the same reaction – treating roxbyite nanorods with 1-DDT – at different temperatures to gain insights into how rapidly the morphological transformation could occur and to determine if the morphologies would differ. At 100 °C, a lower temperature than the 130 °C reaction studied initially, spherical nanoparticles could be accessed within 3 h (instead of 2 h at 130 °C), but at 160 °C, a higher temperature, the transformation took place within 5 min (Figure 3). We then treated the nanorods with other straight chain thiols at 130 °C, including decanethiol (DT) and octadecanethiol (ODT), and found that spherical nanoparticles formed as well (Figure 3c and 3d, respectively). Steric hindrance of ligands on copper sulfide nanorods has been shown previously to impact rod reactivity due to denser surface packing on the sides vs. tips,[41] suggesting that a branched thiol ligand such as t-DDT would behave differently with regards

to particle reshaping than the straight chain thiols. Under the same conditions as for the 1-DDT reaction, the roxbyite nanorods and t-DDT were injected at 130 °C. The rods became shorter and wider with prominent surface facets by 36 h, giving them an ovular shape distinct from the spheres that resulted from 1-DDT treatment (Figure 4b).

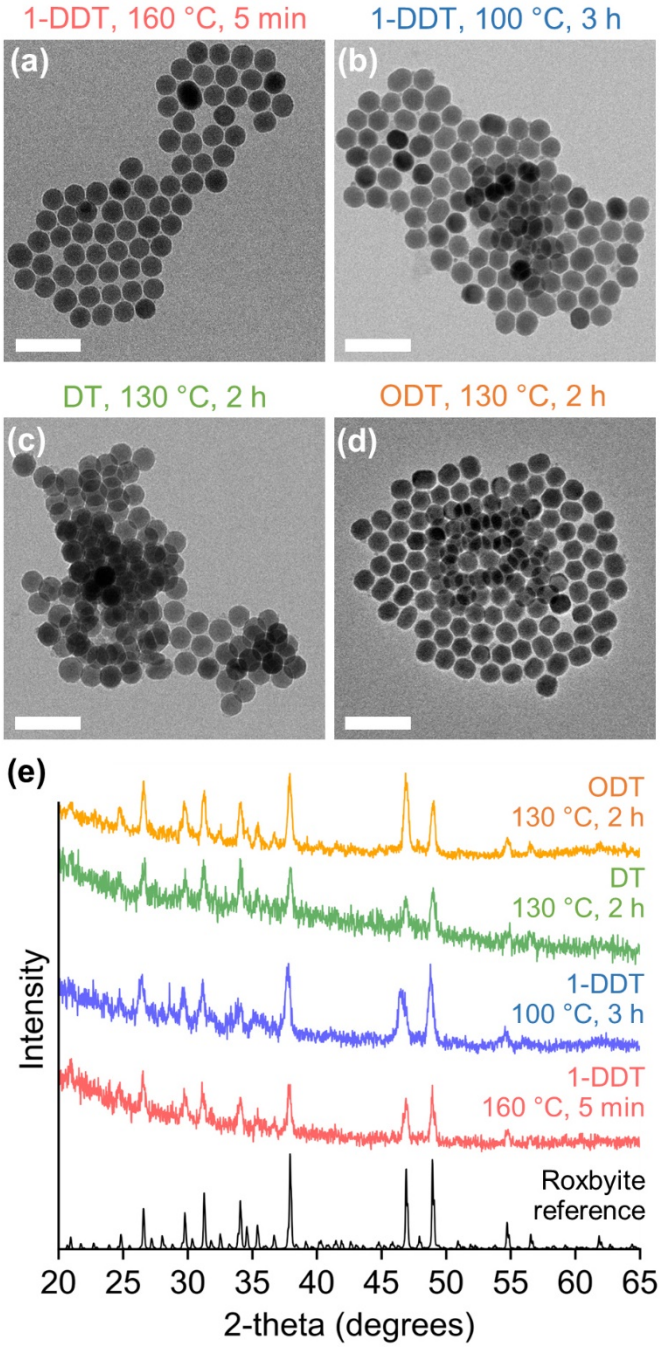

Figure 3. TEM images of the spherical particles that form from $Cu_{1.8}S$ rods treated in (a) 1-dodecanethiol (1-DDT) at 160 °C, (b) 1-DDT at 100 °C (c) 1-decanethiol (DT) at 130 °C, and (d) 1-octadecanethiol (ODT) at 130 °C. Scale bars are 100 nm. (e) Experimental powder XRD patterns of the treated rods, along with a reference pattern for roxbyite $Cu_{1.8}S$.[38]

Unlike with 1-DDT, where temperature impacted only the rate at which particle reshaping occurred without changing the final morphology, the temperature in the t-DDT system did impact nanoparticle morphology, as shown in Figure 4. At a higher temperature of 160 °C, the morphology change relative to the starting nanorods is subtle and does not change beyond 24 hours. The nanorods became slightly shorter and wider with dimensions of 51 ± 4 nm × 23 ± 1 nm, and a conserved volume of $2.1 \times 10^4 \pm 0.4 \times 10^4$ nm^3. At the lower temperatures (110 °C and 90 °C), the nanoparticle morphology appeared to be influenced by etching as evidenced by the appearance of a yellow copper-thiolate solution over the course of the reaction, coupled with an eventual disappearance of the particles.[42,43] The etching behavior of this particular combination of alkylthiol and temperature was found to be reproducible. Alkylthiols have been known to induce etching of metal chalcogenide nanoparticles.[44–46] While it is difficult at this stage to fully understand the origin of this etching behavior, we speculate that there must be a threshold amount of time for the t-DDT to be bound to the surface for it to solvate the Cu^+ cations and allow them (concomitantly with S^{2-} anions) to be removed from the nanoparticle. Lower temperatures would likely facilitate longer residence time for t-DDT to be bound to the surface than higher temperatures, where there would be a more dynamic ligand exchange environment, thereby favoring etching at lower rather than higher temperatures. The final morphology after 24 hours of the nanoparticles reacting with t-DDT at 110 °C were shorter and wider rods with rounded tips. While 90 °C was a sufficiently low temperature to completely etch the particles by 10 hours, stopping the reaction at four hours yielded narrow nanorods with sharp tips. For the resulting 160 °C and 130 °C t-DDT induced products, the XRD patterns show retention of the roxbyite crystal structure, as was seen in the 1-DDT system (Figure S1). The resulting 110 °C and 90 °C t-DDT induced products, that were also influenced by etching, resemble the djurleite phase of copper sulfide, which has a crystal structure that is very closely related to roxbyite (Figure S2).[38,47]

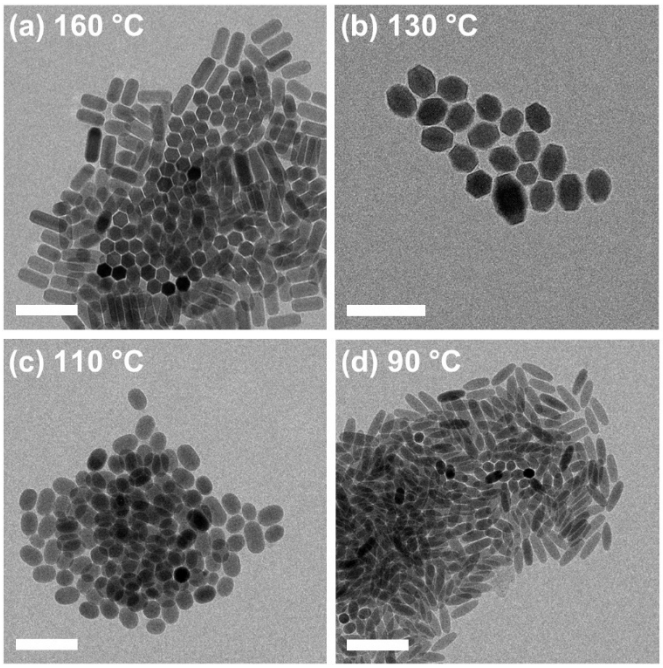

Figure 4. TEM images characterizing the $Cu_{1.8}S$ particle morphologies that form upon treating $Cu_{1.8}S$ rods in t-DDT at (a) 160 °C, (b) 130 °C, (c) 110 °C, and (d) 90 °C. Scale bars are 100 nm.

We speculate that the difference in the temperature dependence of the morphology change for the 1-DDT *vs.* t-DDT systems is due to reactivity. Both 1-DDT and t-DDT are common sulfur reagents in nanoparticle synthesis; however, t-DDT is considered more reactive because of its lower thermolysis temperature of 160 °C compared to 180 °C for 1-DDT in these conditions.[11,27,37] As the injection temperature approaches the decomposition temperature of 160 °C, the t-DDT ligand decomposes, lowering the concentration of t-DDT present in solution. We speculate that less t-DDT present in solution leads to a less pronounced morphology change relative to the product formed at 130 °C.

Having observed the influence of reaction time, reaction temperature, and identity of the thiol ligand on particle reshaping, we also considered the role of nanoparticle morphology. Roxbyite $Cu_{1.8}S$ plates were synthesized (Figure S3a) and subjected to treatment with 1-DDT. The original plates had a diameter of 43 ± 8 nm and a thickness of 13 ± 1 nm with faceted edges. In contrast to the spheres that resulted from thiol-induced reshaping of the nanorods treated with 1-DDT, here, for the nanoplates, the resulting particles were disk shaped with rounded edges, which represents a clear loss of faceting from the starting plates. The particles had a diameter of 45 ± 7 nm and a thickness of 14 ± 1 nm (Figure S3b). These results demonstrate that the morphology after thiol-induced reshaping is dependent upon the morphology of the initial starting nanoparticles, which makes sense because of the crystallographic dependence to reshaping that was detailed in Figure 1. As discussed in Figure 1, the number of closed packed planes decreases as the rod shortens. However, the area of the closed packed planes increases as the rod widens. In the $Cu_{1.8}S$ plates, there are already very few closed packed planes of sulfur stacked in the direction corresponding to the thickness of the plate, while the area of those planes is effectively already maximized on the face of the plate. This could rationalize why the morphology change in the plates is relatively small. Similarly to the case of roxbyite nanorods treated with 1-DDT, the crystal structure was conserved in the final product (Figure S3e).

It is known that treatment with 1-DDT can drive a crystal structure change in covellite (CuS) to form high chalcocite (Cu_2S).[34] This crystal structure change occurs concomitantly with a composition change that is triggered by breaking the disulfide bonds that are present in covellite and then is followed by a small change in morphology from hexagonal plates to thicker, rounded plates. In contrast, our system maintains the roxbyite crystal structure before and after treatment with 1-DDT, which indicates that the precursor and product do not differ in crystal structure or composition. To help validate this key difference between the reactivity of 1-DDT with covellite *vs*. roxbyite, we carried out a control experiment by treating covellite CuS plates with 1-DDT under the same conditions we used for roxbyite $Cu_{1.8}S$. The covellite plates were synthesized by treating the $Cu_{1.8}S$ nanorods with an oleylamine-sulfur complex, which is commonly used in direct nanoparticle synthesis as a sulfur source (Figure S3c).[34] The covellite plates were then treated in 1-DDT at 130 °C for two hours (Figure S3d), identical to the treatment applied to the roxbyite plates. Here, for the covellite system, the plate morphology was retained through the thiol treatment, which contrasts with the conversion to a disk morphology that was observed for the roxbyite plates. For the covellite plates, there was also a change in crystal structure and composition from covellite CuS to digenite $Cu_{1.8}S$, along with a copper metal impurity (Figure S3f). In contrast, the roxbyite plates retained the roxbyite crystal structure and composition ($Cu_{1.8}S$) through the transformation to disks. These experiments emphasize that in the presence of covellite, 1-DDT acts as a reducing agent, breaking the sulfur-sulfur bonds and allowing the crystal phase to change to digenite, as previously reported (Figure S2).[34] Therefore in the covellite system,

1-DDT is chemically facilitating a change in the crystal structure and composition, which is coupled to, and likely helps to cause, the morphology change. However, for the roxbyite system that does not contain disulfide bonds, 1-DDT is not a sufficiently strong reducing agent to change composition, and the crystal structure is maintained (Figure S2).

All of the particle reshaping studies described above have focused on copper sulfides. We also treated wurtzite zinc sulfide (ZnS) with 1-DDT and t-DDT. As can be seen in the TEM images and histograms in Figure 5, treatment with 1-DDT or t-DDT changes neither the size nor the shape of the ZnS nanoparticles, and the corresponding XRD data confirm that the phases remain unchanged as well. The length of the ZnS nanoparticles before and after thiol treatment is consistently 52 ± 3 nm while the width is consistently 20 ± 1 nm. STEM-EDS images of the ZnS nanorods before and after treatment are shown in Figure S4. These data therefore suggest that the particle reshaping may be selective to copper sulfide. To understand the basis for this potential selectivity, we considered the key aspects of the crystal structure, as well as cation vacancies, which are known to enhance diffusion and therefore could be implicated in a particle reshaping pathway that involves material diffusion and migration, as discussed earlier. We first considered the charges of the cations. Roxbyite contains Cu^{+}, while ZnS contains Zn^{2+}. Divalent cation mobilities are much lower than those of monovalent cations, which suggests that $Cu_{1.8}S$ would be much more amenable to reshaping through this pathway than ZnS, as observed.[48,49] Copper cations are also prone to changing oxidation states and would be susceptible to doing so in different ligand environments that have different redox conditions, unlike the Zn^{2+} cation. Lastly, the distorted anion sublattice of $Cu_{1.8}S$ is more likely than ZnS to rearrange during cation exchange, as it must necessarily shift locally to transform to the non-distorted close packed planes in wurtzite.[50]

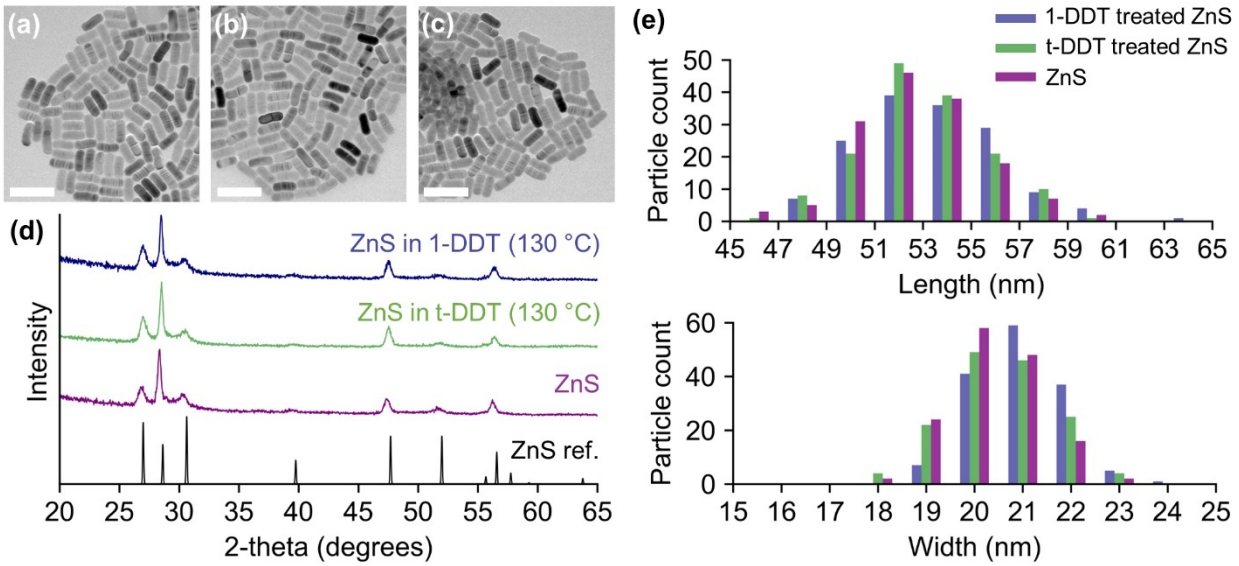

Figure 5. TEM images of (a) ZnS rods obtained through cation exchange of $Cu_{1.8}S$ nanorods, (b) ZnS rods treated with 1-DDT at 130 ºC, and (c) ZnS rods treated with t-DDT at 130 ºC. Scale bars are 100 nm. (d) Experimental powder XRD patterns of the untreated ZnS rods and the 1-DDT and t-DDT treated ZnS rods, along with a reference pattern of wurtzite ZnS.[51] (e) Histograms show the lengths and widths of the ZnS particles.

In addition to the charge consideration, roxbyite (along with several other copper sulfides) contains a high density of cation vacancies in the crystal structure, which imparts high copper

cation mobilities.[36,52] We speculate, based on our hypothesis that the thiol-induced reshaping pathway involves material diffusion and migration, that these cation vacancies play a key role in accelerating the morphology change, similarly to how the cation vacancies in roxbyite help Cu^+ diffuse through the crystal structure to accelerate cation exchange reactions.[26] To test this hypothesis, we treated the roxbyite nanorods with iodine to increase the density of copper cation vacancies, as reaction with I_2 in THF is known to extract Cu^+, leaving behind vacancies.[36,53] This method of increasing the number of vacancies in roxbyite nanorods has been shown to increase cation exchange rates.[36] Changes in vacancy concentrations can be monitored using UV-vis-NIR spectroscopy.[36,53] As copper cations are removed from the nanorods, holes are generated in the valance band, which changes the carrier concentration. This, in turn, increases the localized surface plasmon resonance frequency, thereby blue-shifting the plasmon band.[53–56] Figure 6a, which shows the plasmon band of the untreated roxbyite rods at 1460 nm and the blue-shifted plasmon band of the iodine treated roxbyite rods at 1360 nm, is consistent with a higher concentration of vacancies in the iodine treated rods. Both the untreated and iodine treated nanorods were subjected to treatment with 1-DDT at 110 °C; the lower temperature of 110 ºC (relative to 130 ºC that was used in Figure 1) slowed down the morphology change and allowed us to interrogate its evolution over a longer period of time. TEM images for the untreated and iodine treated nanorods are shown in Figures 6b and 6c, respectively. (Note that some nanorods are oriented upright in the TEM images; these are distinct from the nominally spherical particles, which are significantly wider than the cross section diameters of the vertically-stacked nanorods.) The iodine treated nanorods began to change morphology within 30 minutes while up to 2 hours was required to see a morphology change in the untreated nanorods. The increased vacancy concentration therefore correlated with a faster morphology change, suggesting that the selectivity of the particle reshaping process for roxbyite copper sulfide is due to cation mobilities that are enhanced by vacancies in the crystal structure. Sufficient mobility of the Cu^+ cations appears to be a prerequisite for the observed morphology change.

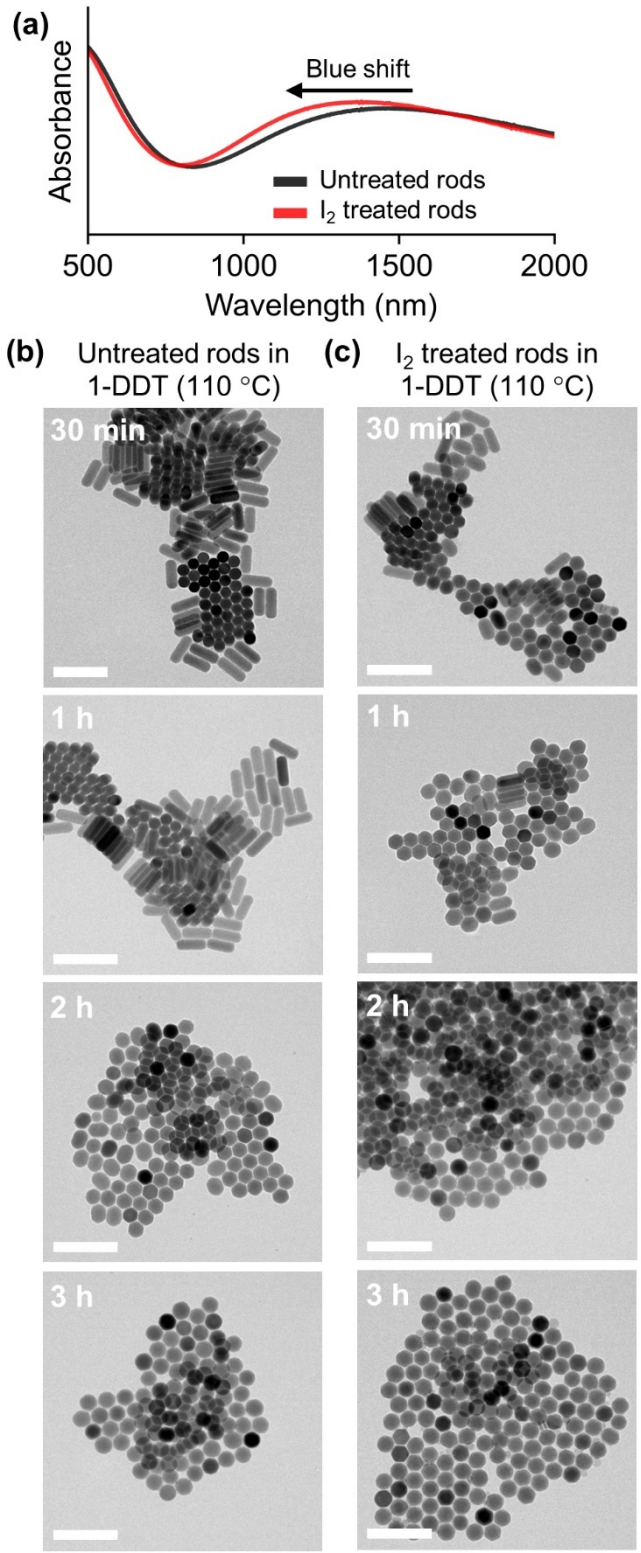

Figure 6. (a) UV-vis-NIR spectrum of $Cu_{1.8}S$ nanorods before and after treatment with I_2. TEM images of aliquots of (b) untreated and (c) I_2 treated $Cu_{1.8}S$ rods in 1-DDT at 110 °C for 3 hours. Scale bars are 100 nm. In the early time point TEM images, some nanorods are oriented upright; these are distinct from the thiol-treated spherical particles, which are significantly wider than the cross-section diameters of the vertically-stacked nanorods.

The observed selectivity for roxbyite copper sulfide suggests that particle reshaping could be localized to the copper sulfide regions of heterostructured metal sulfide nanorods that contain both roxbyite and other metal sulfides, synthesized using multiple sequential partial cation exchange reactions, to create morphologically complex derivatives. Accordingly, half of the Cu^{+} cations in roxbyite nanorods were exchanged with either Co^{2+}, Zn^{2+}, or In^{3+} to form the Janus nanorod derivatives Co_9S_8–$Cu_{1.8}S$, ZnS–$Cu_{1.8}S$ and $CuInS_2$–$Cu_{1.8}S$ that retain the morphology of the roxbyite nanorod precursor.[20] Figure 7 shows TEM images of these nanorods before and after treatment with 1-DDT and t-DDT at 130 °C for 2 hours. Powder XRD characterization identified the materials in the heterostructures (Figures S5-S7) Analysis of the TEM images in Figure 7, as well as the STEM-EDS data (Figure S8-S10), indicates that for all of the reactions, the reshaping is selective to the $Cu_{1.8}S$ regions. Additionally, the morphological modifications to the $Cu_{1.8}S$ regions of the heterostructured nanorods are similar to those of just $Cu_{1.8}S$ nanorods, as were shown in Figures 1. The heterostructure nanorods treated with 1-DDT each have a rounded $Cu_{1.8}S$ region that has shortened along the length of the rod and widened across the rod, tapering at the center of the rod to meet the interface of the other metal sulfide region. The heterostructure nanorods treated with t-DDT also shortened along the length of the rod and widened across the rod, resulting in an elliptically shaped region that tapers at the center of the rod to meet the interface of the other metal sulfide region.

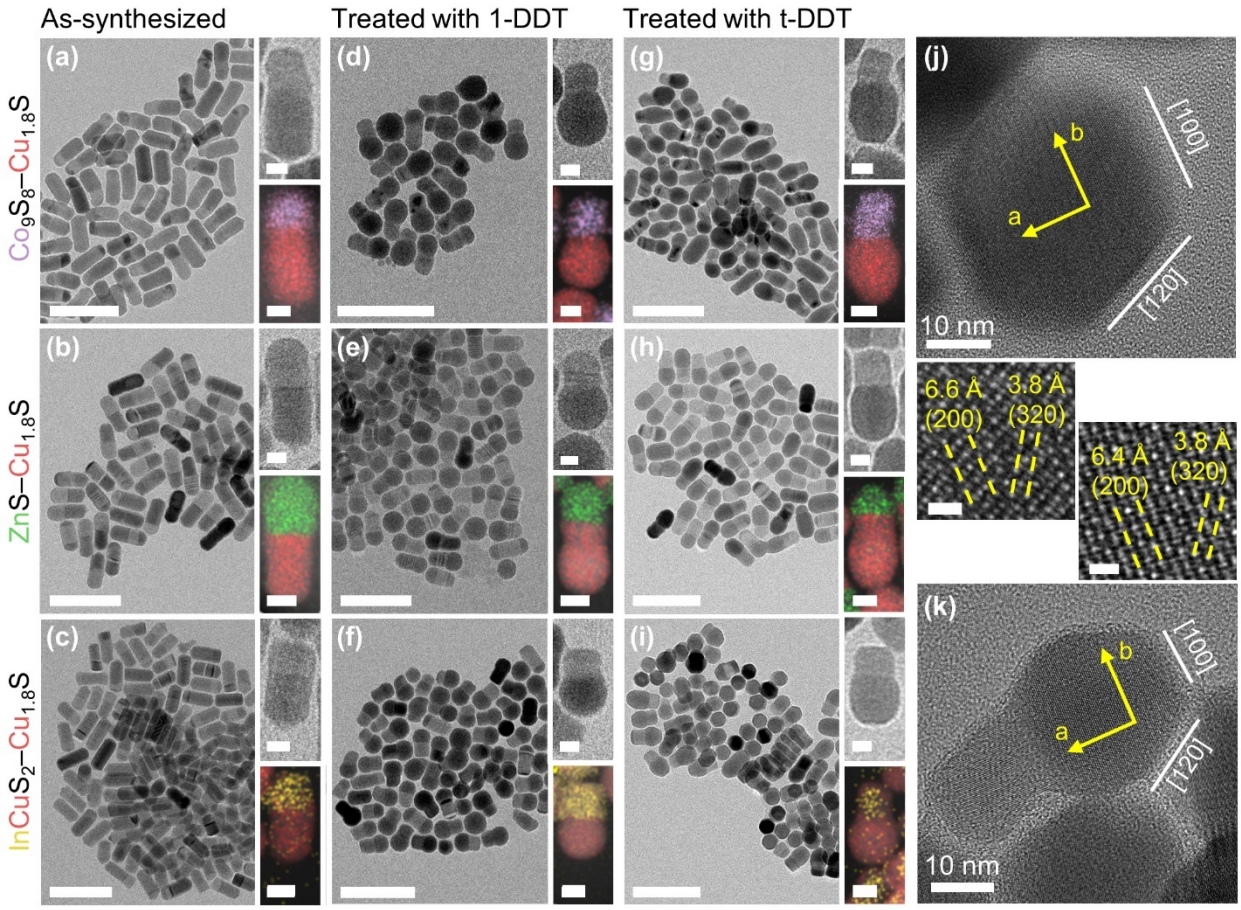

Figure 7. TEM images and corresponding STEM-EDS maps of (a-c) the half-exchanged heterostructured nanorods and after treatment with (d-f) 1-DDT and (g-i) t-DDT at 130 °C for 2 hours. All TEM image scale bars are 100 nm and all STEM-EDS and cropped TEM image scale bars are 10 nm. Cropped particles have $Cu_{1.8}S$ oriented at the

bottom (Cu is represented by red, Co is represented by purple, Zn is represented by green, and In is represented by yellow). HRTEM images of a (j) $Cu_{1.8}S$ rod and (k) Co_9S_8–$Cu_{1.8}S$ heterostructured nanorod treated with 1-DDT at 130 °C for 35 hours. The measured spacings of the (200) and (320) planes closely match the expected values of 6.7 Å and 3.7 Å, respectively.[38] High resolution insets show the $Cu_{1.8}S$ regions and have scale bars of 1 nm.

The Co_9S_8–$Cu_{1.8}S$ heterostructured nanorods were additionally treated with t-DDT at 130 °C for 36 hours for comparison with the previously discussed $Cu_{1.8}S$ rods treated under the same conditions. XRD verified that the $Cu_{1.8}S$ regions in the Co_9S_8–$Cu_{1.8}S$ heterostructured nanorods were indeed roxbyite (Figure S11) and HRTEM was used to find the close packed stacking direction of the $Cu_{1.8}S$ regions in the Co_9S_8–$Cu_{1.8}S$ heterostructured nanorods treated with t-DDT. The stacking direction corresponds to the (200) plane of the roxbyite region, and the exposed facets at the surface are noted as the [100] and [120] family of planes (Figure 7k), and therefore are crystallographically similar to the non-heterostructured $Cu_{1.8}S$ nanorods in Figure 7j. These observations suggest that the morphology transformation in the heterostructured nanorods is the same as in the initial $Cu_{1.8}S$ rods. Application of thiol-induced reshaping of the roxbyite copper sulfide regions in heterostructured nanorods expands the library of complex nanoparticle morphologies that can now be easily accessed with compositional variety.[14,20,25,26,57]

To further expand the applicability of thiol-driven morphology changes for the design of morphologically and compositionally complex nanoparticles, we applied 1-DDT treatment to different types of heterostructured nanorods synthesized using multiple sequential partial cation exchange reactions. In these nanorods, roxbyite copper sulfide is located in a variety of distinct regions. Figure 8 shows TEM images of three different ZnS/$Cu_{1.8}S$ heterostructured nanorod isomers—single tip ZnS–$Cu_{1.8}S$, central band $Cu_{1.8}S$–ZnS–$Cu_{1.8}S$, and double tip ZnS–$Cu_{1.8}S$–ZnS—treated with 1-DDT for 2 h at 130 °C.[20] As expected from the preceding studies that show reshaping occurs only in the $Cu_{1.8}S$ regions, three distinct products form. The single tip ZnS–$Cu_{1.8}S$ nanorods yielded a product with a rounded $Cu_{1.8}S$ region that is similar to the system shown in Figure 4, with the only difference being the extent of partial cation exchange, and therefore the relative ratios of ZnS:$Cu_{1.8}S$ in the nanorods. Similarly, for central band $Cu_{1.8}S$–ZnS–$Cu_{1.8}S$ nanorods, the two terminal $Cu_{1.8}S$ regions rounded, while the central ZnS region remained unchanged. The result of this morphological reshaping was the formation of dumbbell shaped particles. The morphology of the ZnS–$Cu_{1.8}S$–ZnS nanorods changed by widening the central $Cu_{1.8}S$ region, which tapers down to the interface of the two ZnS regions. The morphology change of the double tip rods is less pronounced than that of the other ZnS/$Cu_{1.8}S$ isomers because the $Cu_{1.8}S$ region is constrained between the two ZnS regions. The interface appears to "pin" the morphology, and reshaping occurs only on the outer exposed surfaces.

We then carried out additional Zn^{2+} cation exchange to fully replace all of the remaining $Cu_{1.8}S$ from the ZnS/$Cu_{1.8}S$ heterostructured nanorods with ZnS. This process produced fully ZnS nanorods with sculpted morphologies that ultimately retained the overall morphologies of the partially thiol-reshaped heterostructured nanorods precursors. The fully exchanged ZnS nanoparticles, shown in Figure 8i, derived from the single tip, thiol-reshaped ZnS–$Cu_{1.8}S$ nanorods in Figure 8f are asymmetric with a large, rounded region tapering down to a smaller, rounded region.[20] Likewise, full Zn^{2+} exchange of the thiol-reshaped $Cu_{1.8}S$–ZnS–$Cu_{1.8}S$ dumbbell nanorods in Figure 8h yielded analogously-shaped ZnS dumbbell particles. The ZnS nanoparticles in Figure 8g resulting from the double tip ZnS–$Cu_{1.8}S$–ZnS rods have small, rounded tips that widen towards the center of the particle. The XRD and STEM-EDS images show the full conversion of the heterostructures to ZnS (Figures S12-17). Thiol-induced reshaping therefore

provides a strategy for synthesizing morphologically unique nanoparticles that are inaccessible by both direct colloidal synthesis and traditional cation exchange reactions.

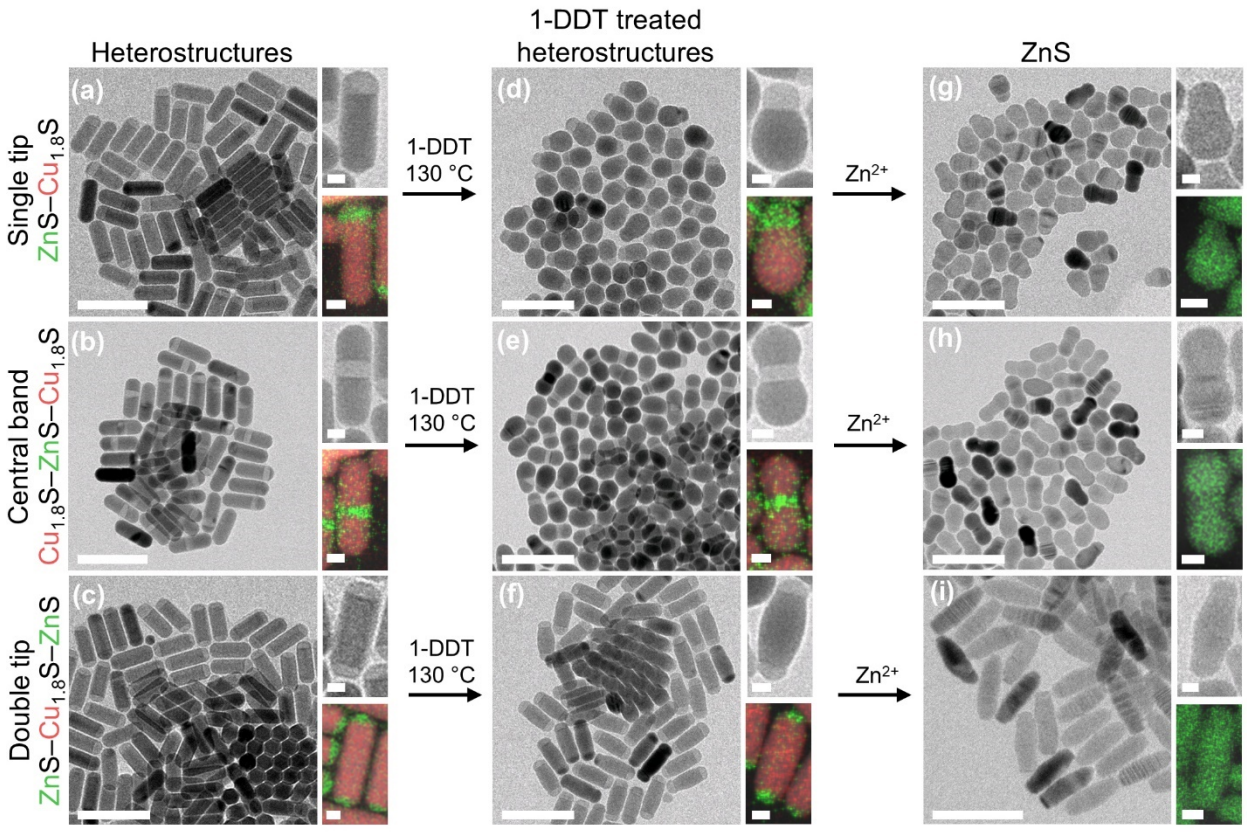

Figure 8. TEM images and corresponding STEM-EDS maps of (a) ZnS–$Cu_{1.8}S$–ZnS double-tip, (b) $Cu_{1.8}S$–ZnS–$Cu_{1.8}S$ central band, and (c) ZnS–$Cu_{1.8}S$ single-tip heterostructured nanorods. TEM images of (d-f) the $Cu_{1.8}S$/ZnS heterostructured nanorods after treatment with 1-DDT at 130 °C for 2 hours and (g-i) after subsequent cation exchange reactions with Zn^{2+}. All wide-view TEM images have scale bars of 100 nm. Cropped TEM and STEM-EDS images have scale bars of 10 nm. STEM-EDS images have Cu represented by red and Zn represented by green.

Conclusions

In summary, we found that treating roxbyite $Cu_{1.8}S$ nanoparticles with the common thiol reagents 1-DDT and t-DDT induces morphology changes that vary depending on time, temperature, and starting nanoparticle morphology; crystal structure and composition also play a role, as covellite CuS behaves differently than roxbyite $Cu_{1.8}S$. Because of this thiol-induced reshaping process, a library of roxbyite copper sulfide nanoparticles with tunable shapes and sizes can now be accessed, including in size ranges that have not previously been achieved using direct synthesis. When applied to heterostructured nanorods that contain roxbyite $Cu_{1.8}S$ regions along with ZnS, Co_9S_8, or $CuInS_2$, the thiol-induced morphology change is observed to be selective for $Cu_{1.8}S$ due to the higher cation mobilities, which are influenced by the charge of the cations and the density of cation vacancies in roxbyite. This regioselective thiol-induced reshaping of heterostructured nanorods produces various distinct types of derivatives having swelled tips and/or central bands. Subsequent cation exchange to fully replace the remaining Cu^+ cations, demonstrated for the transformation of thiol-reshaped ZnS/$Cu_{1.8}S$, produces intricately sculpted ZnS nanoparticles that are morphologically asymmetric. These examples demonstrate the scope of

post-synthetic morphological modifications that are possible, in a controllable and tunable way, by simply heating nanoparticles of roxbyite $Cu_{1.8}S$ (or nanoparticles that contain roxbyite $Cu_{1.8}S$) in either 1-DDT or t-DDT for various amounts of time. As such, these reactions add to the growing toolbox of nanoparticle transformation reactions, leveraging the large number of roxbyite-containing nanoparticles that are accessible *via* partial cation exchange reactions. Given the pathway by which the thiol-reshaping process occurs, it may be possible to apply similar thiol treatment reactions to other classes of copper chalcogenide nanoparticles that have high cation vacancy concentrations, potentially accessing many more nanoparticle morphologies of varying composition.

ASSOCIATED CONTENT

SUPPORTING INFORMATION

Additional experimental details and XRD, TEM, and STEM-EDS data. This material is available free of charge via the Internet at http://pubs.acs.org.

AUTHOR INFORMATION

Corresponding Author

Raymond E. Schaak – *Department of Chemistry*, *Department of Chemical Engineering*, and *Materials Research Institute*, *The Pennsylvania State University, University Park, Pennsylvania 16802, United States*; Email: res20@psu.edu

Authors

Haley L. Young – *Department of Chemistry*, *The Pennsylvania State University, University Park, Pennsylvania 16802, United States*

Connor R. McCormick – *Department of Chemistry*, *The Pennsylvania State University, University Park, Pennsylvania 16802, United States*

Auston G. Butterfield – *Department of Chemistry*, *The Pennsylvania State University, University Park, Pennsylvania 16802, United States*

Enrique D. Gomez – *Department of Chemical Engineering*, *Department of Materials Science and Engineering*, and *Materials Research Institute*, *The Pennsylvania State University, University Park, Pennsylvania 16802, United States*

Notes

The authors declare no competing financial interest.

ACKNOWLEDGMENT

This work was supported by the U.S. National Science Foundation under grant DMR-2210442.

This material is based upon work supported by the National Science Foundation Graduate Research Fellowship Program under Grant No. (DGE1255832). Any opinions, findings, and conclusions or recommendations expressed in this material are those of the author(s) and do not necessarily reflect the views of the National Science Foundation. TEM imaging, X-ray diffraction, and UV-vis-NIR spectroscopy were performed at the Materials Characterization Lab of the Penn State Materials Research Institute. The authors thank Prof. Katherine Plass for helpful discussions.

References

1) Park, J.; Won, Y.; Han, Y.; Kim, H.; Jang, E.; Kim, D. Tuning Hot Carrier Dynamics of InP / ZnSe / ZnS Quantum Dots by Shell Morphology Control. *Small*. **2022**, *18*, 2105492. DOI: 10.1002/smll.202105492
2) Wang, H.; Xie, Y.; Cao, H.; Li, Y.; Li, L.; Xu, Z. Flower-Like Nickel Phosphide Microballs Assembled by Nanoplates with Exposed High-Energy (001) Facets : Efficient Electrocatalyst for the Hydrogen Evolution Reaction. *ChemSusChem*. **2017**, *10*, 4899–4908. DOI: 10.1002/cssc.201701647
3) Choi, H.; Kim, S.; Luther, J. M.; Kim, S.; Shin, D.; Beard, M. C.; Jeong, S. Facet-Specific Ligand Interactions on Ternary $AgSbS_2$ Colloidal Quantum Dots. *Chem. Eur. J.* **2017**, *23*, 17707–17713. DOI:10.1002/chem.201703681
4) Xia, X.; Zeng, J.; Zhang, Q.; Moran, C. H.; Xia, Y. Recent Developments in Shape-Controlled Synthesis of Silver Nanocrystals. J. Phys. Chem C. **2012**, *116*, 21647–21656. DOI: 10.1021/jp306063p
5) Bealing, C. R.; Baumgardner, W. J.; Choi, J. J.; Hanrath, T.; Hennig, R. G. Predicting Nanocrystal Shape through Consideration of Surface-Ligand Interactions. *ACS Nano* **2012**, *6*, 2118–2127. DOI: 10.1021/nn3000466
6) Zhang, Q.; Han, L.; Jing, H.; Blom, D. A.; Lin, Y.; Xin, H. L.; Wang, H. Facet Control of Gold Nanorods. *ACS Nano* **2016**, *10*, 2960–2974. DOI: 10.1021/acsnano.6b00258
7) van Oversteeg, C. H. M.; Oropeza, F. E.; Hofmann, J. P.; Hensen, E. J. M.; de Jongh, P. E.; de Mello Donega, C. Water-Dispersible Copper Sulfide Nanocrystals via Ligand Exchange of 1-Dodecanethiol. *Chem. Mater*. **2019**, *31*, 541-552. DOI: 10.1021/acs.chemmater.8b04614
8) Jiang, X. C.; Chen, W. M.; Chen, C. Y.; Xiong, S. X.; Yu, A. B. Role of Temperature in the Growth of Silver Nanoparticles Through a Synergetic Reduction Approach. *Nanoscale Res Lett.* **2011**, *6*, 1–9. DOI: 10.1007/s11671-010-9780-1
9) Bahena-Martínez, C. J.; Torres-Gómez, N.; Vilchis-Néstor, A. R. Study of the temperature effect on the morphology and structure of ZnS nanoparticles synthesized by hydrothermal method. *MRS Advances.* **2020**, *5*, 3379–3388. DOI: 10.1557/adv.2020.409
10) Al-Hada, N. M.; Kasmani, R. M.; Kasim, H.; Al-Ghaili, A. M.; Saleh, M. A.; Banoqitah, E. M.; Alhawsawi, A. M.; Baqer, A. A.; Liu, J.; Xu, S.; Li, Q.; Noorazlan, A. M.; Ahmed, A. A. A.; Flaifel, M. H.; Paiman, S.; Nazrin, N.; Al-Asbahi, B. A.; Wang, J. The Effect of Precursor Concentration on the Particle Size, Crystal Size, and Optical Energy Gap of $Ce_xSn_{1-x}O_2$ Nanofabrication. *Nanomaterials* **2021**, *11*, 1–14. DOI: 10.3390/nano11082143
11) Zhai, Y.; Shim, M. Effects of Copper Precursor Reactivity on the Shape and Phase of Copper Sulfide Nanocrystals. *Chem. Mater.* **2017**, *29*, 2390–2397. DOI: 10.1021/acs.chemmater.7b00461
12) Robinson, E. H.; Turo, M. J.; Macdonald, J. E. Controlled Surface Chemistry for the Directed Attachment of Copper(I) Sulfide Nanocrystals. *Chem. Mater.* **2017**, *29*, 3854–3857. DOI: 10.1021/acs.chemmater.6b05080
13) Nelson, A.; Ha, D. H.; Robinson, R. D. Selective Etching of Copper Sulfide Nanoparticles and Heterostructures through Sulfur Abstraction: Phase Transformations and Optical Properties. *Chem. Mater*. **2016**, *28*, 8530–8541. DOI: 10.1021/acs.chemmater.6b02764
14) Butterfield, A. G.; Steimle, B. C.; Schaak, R. E. Retrosynthetic Design of Morphologically Complex Metal Sulfide Nanoparticles Using Sequential Partial Cation Exchange and

Chemical Etching. *ACS Materials Lett.* **2020**, *2*, 1106–1114. DOI: 10.1021/acsmaterialslett.0c00287
15) Latham, A. H.; Wilson, M. J.; Schiffer, P.; Williams, M. E. TEM-Induced Structural Evolution in Amorphous Fe Oxide Nanoparticles. *J. Am. Chem. Soc.* **2006**, *128*, 12632–12633. DOI: 10.1021/ja064666q
16) Nakaso, K.; Shimada, M.; Okuyama, K.; Deppert, K. Evaluation of the change in the morphology of gold nanoparticles during sintering. *Aerosol Science*. **2002**, *33*, 1061–1074. DOI: 10.1016/S0021-8502(02)00058-7
17) Chen, L.; Hu, H.; Li, Y.; Chen, R.; Li, G. Flexible tuning of hole-based localized surface plasmon resonance in roxbyite $Cu_{1.8}S$ nanodisks via particle size, carrier density and plasmon coupling. *J. Mater. Sci.* **2020**, *55*, 116–124. DOI: 10.1007/s10853-019-03923-9
18) Chen, L.; Sakamoto, M.; Sato, R.; Teranishi, T. Determination of a localized surface plasmon resonance mode of Cu_7S_4 nanodisks by plasmon coupling. *Faraday Discuss.* **2015**, *181*, 355–364. DOI: 10.1039/C4FD00239C
19) Li, Z.; Saruyama, M.; Asaka, T.; Tatetsu, Y.; Teranishi, T. Determinants of crystal structure transformation of ionic nanocrystals in cation exchange reactions. *Science* **2021**, *373*, 332–337. DOI: 10.1126/science.abh2741
20) Fenton, J. L.; Steimle, B. C. Tunable intraparticle frameworks for creating complex heterostructured nanoparticle libraries. *Science* **2018**, *360*, 513–517.
21) Goel, S.; Chen, F.; Cai, W. Synthesis and Biomedical Applications of Copper Sulfide Nanoparticles: From Sensors to Theranostics. *Small* **2014**, *10*, 631–645. DOI: 10.1002/smll.201301174
22) Wang, L.; Ma, X.; Cai, K.; Li, X. Morphological effect of copper sulfide nanoparticles on their near infrared laser activated photothermal and photodynamic performance. *Mater. Res. Express*. **2019**, *6*, 105406. DOI: 10.1088/2053-1591/ab3a01
23) Liu, M.; Liu, Y.; Gu, B.; Wei, X.; Xu, G.; Wang, X.; Swihart, M. T.; Yong, K. T. Recent advances in copper sulphide-based nanoheterostructures. *Chem. Soc. Rev*. **2019**, *48*, 4950–4965. DOI: 10.1039/c8cs00832a
24) De Trizio, L.; Manna, L. Forging Colloidal Nanostructures via Cation Exchange Reactions. *Chem. Rev.* **2016**, *116*, 10852–10887. DOI: 10.1021/acs.chemrev.5b00739
25) Fenton, J. L.; Steimle, B. C.; Schaak, R. E. Exploiting Crystallographic Regioselectivity to Engineer Asymmetric Three-Component Colloidal Nanoparticle Isomers Using Partial Cation Exchange Reactions. *J. Am. Chem. Soc.* **2018**, *140*, 6771–6775. DOI: 10.1021/jacs.8b03338
26) Steimle, B. C.; Fenton, J. L.; Schaak, R. E. Rational construction of a scalable heterostructured nanorod megalibrary. *Science* **2020**, *367*, 418–424. DOI: 10.1126/science.aaz1172
27) Kruszynska, M.; Borchert, H.; Bachmatiuk, A.; Rummeli, M. H.; Buchner, B.; Parisi, J.; Kolny-Olesiak, J. Size and Shape Control of Colloidal Copper(I) Sulfide Nanorods. *ACS Nano* **2012**, *6*, 5889–5896.
28) Liu, Y.; Liu, M.; Swihart, M. T. Shape Evolution of Biconcave Djurleite $Cu_{1.94}S$ Nanoplatelets Produced from $CuInS_2$ Nanoplatelets by Cation Exchange. *J. Am. Chem. Soc.* **2017**, *139*, 18598–18606. DOI: 10.1021/jacs.7b09577
29) Fleming, D. A.; Thode, C. J.; Williams, M. E. Triazole Cycloaddition as a General Route for Functionalization of Au Nanoparticles. *Chem. Mater*. **2006**, *18*, 2327–2334. DOI: 10.1021/cm060157b

30) Ellis, R. G.; Turnley, J. W.; Rokke, D. J.; Fields, J. P.; Alruqobah, E. H.; Deshmukh, S. D.; Kisslinger, K.; Agrawal, R. Hybrid Ligand Exchange of $Cu(In,Ga)S_2$ Nanoparticles for Carbon Impurity Removal in Solution-Processed Photovoltaics. *Chem. Mater*. **2020**, *32*, 5091–5103. DOI: 10.1021/acs.chemmater.0c00966
31) Rucareanu, S.; Maccarini, M.; Shepherd, J. L.; Lennox, R. B. Polymer-capped gold nanoparticles by ligand-exchange reactions. *J. Mater. Chem*. **2008**, *18*, 5830–5834. DOI: 10.1039/b806375c
32) Kong, W.; Sun, T.; Chen, B.; Chen, X.; Ai, F.; Zhu, X.; Li, M.; Zhang, W.; Zhu, G.; Wang, F. A General Strategy for Ligand Exchange on Upconversion Nanoparticles. *Inorg. Chem*. **2017**, *56*, 872–877. DOI: 10.1021/acs.inorgchem.6b02479
33) Arora, D.; Tan, H. R.; Wu, W. Y.; Chan, Y. 2D-Oriented Attachment of 1D Colloidal Semiconductor Nanocrystals via an Etchant. *Nano Letters*. **2022**, *22*, 942–947. DOI: 10.1021/acs.nanolett.1c03680
34) Liu, Y.; Liu, M.; Swihart, M. T. Reversible Crystal Phase Interconversion between Covellite CuS and High Chalcocite Cu_2S Nanocrystals. *Chem. Mater.* **2017**, *29*, 4783–4791. DOI: 10.1021/acs.chemmater.7b00579
35) Tang, A.; Qu, S.; Li, K.; Hou, Y.; Teng, F.; Cao, J.; Wang, Y.; Wang, Z. One-pot synthesis and self-assembly of colloidal copper(I) sulfide nanocrystals. *Nanotechnology.* **2010**, *21*, 285602. DOI: 10.1088/0957-4484/21/28/285602
36) Le, H. K. D.; Xiong, H.; Page, B. A.; Garcia-Herrera, L. F.; McAllister, H. P.; Li, B. C.; Wang, H.; Plass, K. E. Effects of I_2 on $Cu_{2-x}S$ Nanoparticles: Enabling Cation Exchange but Complicating Plasmonics. *ACS Mater. Lett.* **2020**, *2*, 140–146. DOI: 10.1021/acsmaterialslett.9b00402
37) Chen, L.; Hu, H.; Chen, Y.; Li, Y.; Gao, J.; Li, G. Sulfur Precursor Reactivity Affecting the Crystal Phase and Morphology of $Cu_{2-x}S$ Nanoparticles. *Chem. Eur. J.* **2020**, *27*, 1057–1065. DOI: 10.1002/chem.202003760
38) Mumme, W. G.; Gable, R. W.; Petricek, V. The Crystal Structure of Roxbyite, $Cu_{58}S_{32}$. *Canadian Mineralogist* **2012**, *50*, 423–430. DOI: 10.3749/canmin.50.2.423
39) Turo, M. J.; Macdonald, J. E. Crystal-Bound vs Surface-Bound Thiols on Nanocrystals. *ACS Nano* **2014**, *8*, 10205–10213. DOI: 10.1021/nn5032164
40) Song, D. K.; Lenggoro, I. W.; Hayashi, Y.; Okuyama, K.; Kim, S. S. Changes in the Shape and Mobility of Colloidal Gold Nanorods with Electrospray and Differential Mobility Analyzer Methods. *Langmuir* **2005**, *21*, 10375–10382. DOI: 10.1021/la0513196
41) Zhai, Y.; Flanagan, J. C.; Shim, M. Lattice Strain and Ligand Effects on the Formation of $Cu_{2-x}S$/I-III-VI_2 Nanorod Heterostructures through Partial Cation Exchange. *Chem. Mater*. **2017**, *29*, 6161–6167. DOI: 10.1021/acs.chemmater.7b02392
42) Ding, X.; Zou, Y.; Jiang, J. Au–Cu_2S heterodimer formation via oxidization of AuCu alloy nanoparticles and *in situ* formed copper thiolate. *J. Mater. Chem*. **2012**, *22*, 23169–23174. DOI: 10.1039/c2jm34916g
43) Steimle, B. C.; Fagan, A. M.; Butterfield, A. G.; Lord, R. W.; McCormick, C. R.; Domizio, G. A. D.; Schaak, R. E. Experimental Insights into Partial Cation Exchange Reactions for Synthesizing Heterostructured Metal Sulfide Nanocrystals. *Chem. Mater.* **2020**, *32* 5461–5482. DOI: 10.1021/acs.chemmater.0c01388
44) Chen, D.; Zhang, H.; Li, Y.; Pang, Y.; Yin, Z.; Sun, H.; Zhang, L.; Wang, S.; Saunders, M.; Barker, E.; Jia, G. Spontaneous Formation of Noble- and Heavy-Metal-Free Alloyed Semiconductor Quantum Rods for Efficient Photocatalysis. *Adv. Mater*. **2018**, *30*,

1803351. DOI: 10.1002/adma.201803351
45) Kuno, J.; Kawai, T.; Nakashima, T. The effect of surface ligands on the optical activity of mercury sulfide nanoparticles. *Nanoscale*. **2017**, *9*, 11590–11595. DOI: 10.1039/c7nr02603j
46) Chen, S.; Tang, T.; Huang, B.; Liu, F.; Cui, R.; Zhang, M.; Sun, T. Thiolate Etching Route for the Ripening of Uniform Ag_2Te Quantum Dots Emitting in the Second Near-Infrared Window: Implication for Noninvasive *In Vivo* Imaging. *ACS Appl. Nano Mater*. **2022**, *5*, 3415–3421. DOI: 10.1021/acsanm.1c04005
47) Evans, H. T. The Crystal Structures of Low Chalcocite and Djurleite. *Z. Kristallogr*. **1979**, *150*, 299-320. DOI: 10.1524/zkri.1979.150.14.299
48) Sotoudeh, M.; Groß, A. Descriptor and Scaling Relations for Ion Mobility in Crystalline Solids. *JACS Au* **2022**, *2*, 463–471. DOI: 10.1021/jacsau.1c00505
49) Tchitchekova, D. S.; Monti, D.; Johansson, P.; Bardé, F.; Randon-Vitanova, A.; Palacín, M. R.; Ponrouch, A. On the Reliability of Half-Cell Tests for Monovalent (Li^+, Na^+) and Divalent (Mg^{2+}, Ca^{2+}) Cation Based Batteries. *J. Electrochem. Soc*. **2017**, *164*, A1384–A1392. DOI: 10.1149/2.0411707jes
50) Butterfield, A. G.; Alameda, L. T.; Schaak, R. E. Emergence and Control of Stacking Fault Formation during Nanoparticle Cation Exchange Reactions. *J. Am. Chem. Soc.* **2021**, *143*, 1779–1783. DOI: 10.1021/jacs.0c13072
51) Xu, Y. N.; Ching, W. Y. Electronic, Optical, and Structural Properties of Some Wurtzite Crystals. *Phys. Rev. B.* **1993**, *48*, 4335–4351. DOI: 10.1103/PhysRevB.48.4335
52) Elimelech, O.; Liu, J.; Plonka, A. M.; Frenkel, A. I.; Banin, U. Size Dependence of Doping by a Vacancy Formation Reaction in Copper Sulfide Nanocrystals. *Angew. Chem. Int. Ed*. **2017**, *56*, 10335–10340. DOI: 10.1002/anie.201702673
53) Jain, P. K.; Manthiram, K.; Engel, J. H.; White, S. L.; Faucheaux, J. A.; Alivisatos, A. P. Doped Nanocrystals as Plasmonic Probes of Redox Chemistry. *Angew. Chem., Int. Ed*. **2013**, *52*, 13671–13675. DOI: 10.1002/anie.201303707
54) Zhao, Y.; Pan, H.; Lou, Y.; Qiu, X.; Zhu, J.; Burda, C. Plasmonic $Cu_{2-x}S$ Nanocrystals: Optical and Structural Properties of Copper-Deficient Copper(I) Sulfides. *J. Am. Chem. Soc*. **2009**, *131*, 4253–4261. DOI: 10.1021/ja805655b
55) Xie, Y.; Riedinger, A.; Prato, M.; Casu, A.; Genovese, A.; Guardia, P.; Sottini, S.; Sangregorio, C.; Miszta, K.; Ghosh, S.; Pellegrino, T.; Manna, L. Copper Sulfide Nanocrystals with Tunable Composition by Reduction of Covellite Nanocrystals with Cu^+ Ions. *J. Am. Chem. Soc*. **2013**, *135*, 17630–17637. DOI: 10.1021/ja409754v
56) Luther, J. M.; Jain, P. K.; Ewers, T.; Alivisatos, A. P. Localized surface plasmon resonances arising from free carriers in doped quantum dots. *Nature Mater.,* **2011**, *10*, 361–366. DOI: 10.1038/nmat3004
57) Schaak, R. E.; Steimle, B. C.; Fenton, J. L. Made-to-Order Heterostructured Nanoparticle Libraries. *Acc. Chem. Res*. **2020**, *53*, 2558–2568. DOI: 10.1021/acs.accounts.0c00520

Table of Contents Graphic